

Cosmology in the dark: On the importance of source population models for gravitational-wave cosmology

S. Mastrogiovanni,¹ K. Leyde,¹ C. Karathanasis,² E. Chassande-Mottin,¹

D. A. Steer,¹ J. Gair,³ A. Ghosh,⁴ R. Gray,⁵ S. Mukherjee,^{6, 7, 8} and S. Rinaldi^{9, 10}

¹*Université de Paris, CNRS, Astroparticule et Cosmologie (APC), F-75013 Paris, France*

²*Institut de Física d'Altes Energies (IFAE), Barcelona Institute of Science and Technology, Barcelona, Spain*

³*Max Planck Institute for Gravitational Physics (Albert Einstein Institute), Am Mühlenberg 1, Potsdam 14476, Germany*

⁴*Ghent University, Proeftuinstraat 86, 9000 Gent, Belgium*

⁵*SUPA, University of Glasgow, Glasgow G12 8QQ, United Kingdom*

⁶*Gravitation Astroparticle Physics Amsterdam (GRAPPA),*

Anton Pannekoek Institute for Astronomy and Institute for Physics,

University of Amsterdam, Science Park 904, 1090 GL Amsterdam, The Netherlands

⁷*Institute Lorentz, Leiden University, PO Box 9506, Leiden 2300 RA, The Netherlands*

⁸*Delta Institute for Theoretical Physics, Science Park 904, 1090 GL Amsterdam, The Netherlands*

⁹*Dipartimento di Fisica "E. Fermi", Università di Pisa, I-56127 Pisa, Italy*

¹⁰*INFN, Sezione di Pisa, I-56127 Pisa, Italy*

(Dated: June 25, 2022)

Knowledge about the shape of the mass spectrum of compact stars helps in breaking the degeneracy between the mass and redshift of the gravitational wave (GW) sources and can be used to infer cosmological parameters in the absence of redshift measurements obtained from electromagnetic observations. In this paper we study the achievable accuracy and the limits of this approach. We perform cosmological inference from GW data assuming parametric compact binary population models. We consider two representative models for the mass spectrum, namely a power-law model between two hard cut-offs at a minimum and maximum mass (m_{\min} and m_{\max} respectively), and a similar model combined with a Gaussian peak. Both models exhibit characteristic scales that allow an indirect estimate of the source redshift. In the case of the LIGO-Virgo detector network with current and future sensitivities we perform the analysis of an extensive set of simulated data using a hierarchical Bayesian scheme that jointly fit the source population and cosmological parameter. We also re-analyse the LIGO-Virgo O2 data. Those analyses all evidence the tight interplay between source population and cosmological parameters and the influence of initial assumptions formulated on the ones or the others. We find that: (i) the upper cut-off m_{\max} and the position of the Gaussian peak display the largest correlation with the cosmological parameters; (ii) incorrect population models may bias the Hubble constant estimate by 40%, or incorrect value for $\Omega_{m,0}$ may lead a significant bias on H_0 ; (iii) the estimates enter the large sample regime with asymptotic normality and $1/\sqrt{N}$ error decay from $N \sim 200$ GW events. Overall, our results suggest that the inference on source population and cosmological parameters should be addressed *jointly* and not separately as it is in most studies so far.

I. INTRODUCTION

Gravitational waves (GWs) [1, 2] from compact binary mergers are often referred to as “*standard sirens*”, in analogy with the term “*standard candles*” coined for SNIa, thus underlining their role for cosmology. From the GW signal it is possible to directly estimate the source luminosity distance d_L [3, 4]. When combined with the redshift of the host galaxy, this estimate can be used to measure cosmological parameters and thus probe the expansion history of the universe.

Probing the expansion history of the universe is crucial to resolve open issues in the standard cosmological model, such as the nature of dark energy and the tension in the values of the Hubble constant H_0 i.e. the expansion rate of the Universe today, obtained from observations at early and late cosmological epochs [5–8].

GWs detected by the LIGO and Virgo experiments [9, 10] have been used to infer H_0 using various approaches and data sets. A first approach [4, 11] is to

obtain the source redshift by locating the host galaxy thanks to an electromagnetic counterpart to the GW signal. This approach has so far been applied in two cases. The measurement $H_0 = 70^{+19}_{-8} \text{ km Mpc}^{-1} \text{ s}^{-1}$ in [12, 13] was obtained after the observation of the *kilonova* optical transient that allowed the galaxy hosting the binary neutron-star (BNS) GW170817 to be pinpointed [14]. Similarly, the optical transient [15] tentatively associated to the binary black hole event GW190521 [16, 17] led to $H_0 = 48^{+24}_{-10} \text{ km Mpc}^{-1} \text{ s}^{-1}$ [18, 19]. From GW sources with electromagnetic counterparts, it is also possible to test the general theory of relativity from GW propagation [20]. In order to make an accurate measurements of cosmological parameters and testing general theory of relativity, it is also crucial to correct for peculiar velocity of galaxies which is mainly essential for the GW sources situated at low redshift [21, 22].

A second approach [11] consists in establishing a statistical association between the source, and those galaxies in a catalog that match the source sky location and lu-

minosity distance as inferred from the GW data. This is well suited to binary black hole (BBH) mergers as electromagnetic counterparts are not expected in this case (So far, there are no clear and robust discovery of a counterpart). A proof of principle application of this approach has been applied to GW170817, ignoring the counterpart, finding $H_0 = 77^{+37}_{-18} \text{ km Mpc}^{-1} \text{ s}^{-1}$ [23]. This approach has been applied to the BBH signals detected during the first and second observing runs of Advanced LIGO and Virgo [2, 24, 25] leading to a value of $H_0 = 69^{+16}_{-8} \text{ km Mpc}^{-1} \text{ s}^{-1}$ when combined with the BNS counterpart measurement. An analysis of the asymmetric mass ratio event GW190814 [26] detected during the first half of observing run 3 [27] resulted in the estimate $H_0 = 70^{+17}_{-8} \text{ km Mpc}^{-1} \text{ s}^{-1}$. A more recent result using also O3a events finds $H_0 = 70^{+11}_{-7} \text{ km Mpc}^{-1} \text{ s}^{-1}$ [28].

Several recent studies characterize the future prospects for both approaches in the context of the upcoming observing runs (O4 and O5) for Advanced LIGO and Advanced Virgo, and for the 3rd generation detectors such as the Einstein Telescope (ET). They all concur on the rapid increase in difficulty for obtaining reliable and precise redshift measurements from electromagnetic observations as the GW sensitivity improves and the average distance of the detected events increases. The search for electromagnetic counterparts becomes more challenging [29, 30]: sources at greater distances have dimmer counterparts and a larger number of potential host galaxies. Also the lack of completeness of galaxy surveys to high redshifts prevents the use of the statistical association for the large fraction of BBHs that will be observed by the future GW detectors [31]. Another way to infer the redshift of the GW sources is to explore the spatial clustering scale between the galaxies and GW sources. By cross-correlating GW sources with galaxies, we can infer the clustering redshift that can enable to measure the expansion history along with the GW bias parameters which captures the evolution of astrophysical population of BBHs with redshift [32–35]. The cross-correlation technique can also be used to test the general theory of relativity from GW propagation [36].

These limitations have motivated the development of alternative methods to obtain the source redshift solely from GWs. One possibility is to rely on assumptions about the masses of the compact stars in the source frame [37–39]. The binary component masses inferred directly from the GW signal M_z are *redshifted*, and thus differ from the source-frame mass M by a $(1+z)$ factor as $M_z = (1+z)M$. Therefore the source redshift can be deduced from the measured detector-frame mass and a statistical estimate of the source-frame mass based on a belief about its distribution. This requires solid prior knowledge of the mass distribution, or that it can be inferred from available data.

To be effective, this method requires the presence of features in the mass distribution that break scale invariance. Discontinuities in the mass distribution defines typical source-frame mass scales associated with accumula-

tion points (narrow peaks) or sudden extinction (sharp breaks), that can be leveraged to infer the redshift of those GW events falling close-by, through a comparison with their observed detector mass. This idea has been explored in several works, which explore how one can constraint mass distributions and cosmologies together.

In [38] the authors propose exploiting the narrow BNS component mass distribution (normal distribution with a few percent scatter) [40, 41] to constrain H_0 within 10% using hundreds of LIGO and Virgo GW events. Assuming H_0 , $\Omega_{m,0}$ and $\Omega_{k,0}$ are known at the sub-percent accuracy, reference [39] follows the same idea to constrain the equation of state of dark matter from ET observations.

The mass distribution of black holes is expected to be shaped by various processes, in particular by pair-instability supernovae (PISN) [42]. PISN is expected to lead to a depletion in the black hole mass distribution in a range from ~ 50 to $\sim 120 M_\odot$, that is often referred to as “mass gap”. From the determination of the low end of the mass gap [43] shows it is possible to put a $\sim 6.1\%$ constraint on $H(z=0.8)$ after one year at design sensitivity for Advanced LIGO and Virgo. Reference [44] explores the same idea with 3rd generation detectors finding that, after a year of ET observations, it will be possible to measure H_0 at the percent level. Similarly, [45] proposes to use the high end of the PISN mass gap (i.e., the observation of intermediate-mass black hole binaries) to estimate H_0 at $\lesssim 20\%$ accuracy and down to $\sim 3\%$ in the most optimistic scenario with ET.

Along the same lines of the aforementioned works, this paper focuses on BBHs and elaborates on the contributions of the previous paragraph. The proposed approach inherently couples the inference of source population properties (such as the mass distribution) and of cosmological parameters, and the systematics that fixing one or the another might introduce. We provide evidence that *there are gains in robustness and accuracy to be expected by doing these two types of analyses jointly* and not separately nor sequentially. To this end, we identify what systematics in the estimation of cosmological parameters from GW data are introduced by source population assumptions. The study concentrates on the near term and the upcoming LIGO and Virgo observing runs.

In Sec. II we present a joint inferential scheme for both cosmology and source population. In Sec. III we highlight which are the most important source population parameters for GW cosmology, assuming current detector sensitivities. In Sec. IV we discuss in more detail possible systematics (on the estimation of cosmological parameters) that can be introduced by population assumptions. Then in Sec. V we discuss the impact of population assumptions on the estimation of H_0 using the 6 high-SNR BBHs of the GWTC-1 catalog. We also present the result obtained with a complete “end-to-end” analysis that gives a hint of what can be achieved with the upcoming observing run O4. Finally we draw our conclusions in Sec. VI.

II. HIERARCHICAL BAYESIAN ANALYSIS

In this section, we introduce our notation and outline the scheme for jointly inferring cosmological and source population parameters.

A. Notation and definition of source population models

We denote by θ the parameters of individual sources: most important amongst these for the present analysis are the source-frame masses, $m_{1/2,s}$, of the two binary components, and the cosmological redshift z . The set of hyperparameters describing the entire BBH population are denoted by Λ_m . Together with the cosmological parameters such as the Hubble constant H_0 and the present-day fraction of matter density $\Omega_{m,0}$ for a flat Λ CDM Universe, those parameters induce priors on the distribution of component masses and source redshift

$$p_{\text{pop}}(\theta|\Lambda_m, H_0, \Omega_{m,0}) = C p(m_{1,s}, m_{2,s}|\Lambda_m) \times \frac{dV_c}{dz}(H_0, \Omega_{m,0})(1+z)^{\gamma-1} \quad (1)$$

Here $\frac{dV_c}{dz}(H_0, \Omega_{m,0}) = \frac{4\pi c(1+z)^2 D_A^2}{H(z)}$ is the differential comoving volume which is related to the angular diameter distance D_A , and expansion history of the Universe $H(z)$, the factor of $(1+z)$ in Eq. 1 is the standard time dilatation between source and detector frame clocks, and $p(m_{1,s}, m_{2,s}|\Lambda_m)$ describes the source-frame mass distribution. The power-law index γ characterizes the merger rate evolution with redshift [46]: a null value of γ corresponds to a constant merger rate in the comoving volume, while a positive value corresponds to higher rates at higher redshift. Finally the constant C ensures proper normalization of the probability distribution to unity.

We use two models for the source-frame mass spectrum that were previously implemented in [47, 48]. The first is simple power-law model, labelled PL, in which the prior on the first component mass $m_{1,s}$ is a power law with index $(-\alpha)$ and lower and upper cutoffs at m_{\min} and m_{\max} respectively. The second component mass is distributed according to a power law with index β between m_{\min} and $m_{1,s}$. This simple model is completely determined by four parameters, i.e., m_{\max} , m_{\min} , α and β and it is characteristic of the standard “isolated” formation scenario, in which BBHs form in isolated binaries and are subject to the PISN.

The second more complex model is labelled PLG. Here the first component mass follows the same PL model as above with the addition of a Gaussian peak with mean μ_g and variance σ_g^2 . The proportion of events that arise from the Gaussian peak is governed by the parameter λ_g (when $\lambda_g = 0$, the model PLG reduces to PL.). The second mass component is drawn as in the previous model. In addition, this model also includes a tapering factor δ_m for the low mass cut-off as described in [47, 48]. The

model PLG is thus completely determined by six parameters. It is able to capture formation channels such as hierarchical formation in dense globular clusters. The Gaussian peak then represents a pile up of BBHs e.g., due to the presence of PISN.

Current data [47, 48] suggest that the BBH formation is a mixture of the isolated and hierarchical formation channel and is thus better fitted by a PLG model.

B. Basics of the inference scheme

We now present the general framework for joint population and cosmological inference. To keep the notation simple, we collect all (cosmological and source population) hyper-parameters in a single variable $\Lambda = \{\Lambda_m, H_0, \Omega_{m,0}\}$. Given a set of N_{obs} GW detections associated with the data $\{x\} = (x_1, \dots, x_{\text{obs}})$, the posterior on Λ can be expressed as [49–51]

$$p(\Lambda|\{x\}, N_{\text{obs}}) \propto p(\{x\}, N_{\text{obs}}|\Lambda)p(\Lambda), \quad (2)$$

where $p(\Lambda)$ is a prior on the hyper-parameters. The term $p(\{x\}, N_{\text{obs}}|\Lambda)p(\Lambda)$ can be expanded as

$$p(\{x\}, N_{\text{obs}}|\Lambda)p(\Lambda) = p(N_{\text{obs}}|\Lambda) \prod_i^{N_{\text{obs}}} p(x_i|N_i, \Lambda), \quad (3)$$

where the term $p(N_{\text{obs}}|\Lambda)$ is a Poisson’s distribution that relates the number of events observed with the number of events expected. Since we are not interested in rate estimation in this work, we analytically marginalize over the total number of expected events by setting a scale-free prior [46, 49], which is also linked to the merger rates.

The term $p(x_i|N_i, \Lambda)$ can be rewritten using Bayes theorem as

$$p(x_i|N_i, \Lambda) = \frac{p(N_i|x_i, \Lambda)p(x_i|\Lambda)}{p(N_i|\Lambda)}, \quad (4)$$

where $p(N_i|x_i, \Lambda)$ is the probability for detecting the event i given the data x_i and a set of cosmological parameters Λ . This evaluates to unity [49], since we actually detected this event.

The likelihood of the GW event $p(x_i|\Lambda)$ given the population parameters can be factorized using the single source parameters θ as

$$p(x_i|\Lambda) = \int p(x_i|\Lambda, \theta)p_{\text{pop}}(\theta|\Lambda)d\theta, \quad (5)$$

where $p_{\text{pop}}(\theta|\Lambda)$ is the population-induced prior of Eq. 1.

The denominator $p(N_i|\Lambda)$ is the probability of detecting the event given a set of cosmological parameters. This is a normalization factor of the likelihood $p(x_i|\Lambda)$ and it describes what is usually referred to as *selection effects* [49, 51]. This term can be written as an integral over every possible realization of detectors’ data that will pass the detection threshold

$$p(N_i|\Lambda) = \int_{x>\text{thr}} \int p(x|\theta, \Lambda)p_{\text{pop}}(\theta|\Lambda)d\theta dx. \quad (6)$$

The detection rule usually consists in a threshold on the signal-to-noise (SNR) ratio (or equivalently on the false alarm rate). The integral can then be written as [49]

$$p(N_i|\Lambda) = \int p_{\text{det}}(\theta, \Lambda) p_{\text{pop}}(\theta|\Lambda) d\theta, \quad (7)$$

where $p_{\text{det}}(\theta, \Lambda)$ is the probability of detecting the source with parameters θ and assuming the population and cosmological hyper-parameters Λ . By substituting in Eq. 2 the terms in Eqs. 7-5 we obtain the posterior on the source population and cosmological hyper-parameters

$$p(\Lambda|\{x\}, N_{\text{obs}}) \propto p(\Lambda) \prod_i^N \frac{\int p(x_i|\Lambda, \theta) p_{\text{pop}}(\theta|\Lambda) d\theta}{\int p_{\text{det}}(\theta, \Lambda) p_{\text{pop}}(\theta|\Lambda) d\theta}. \quad (8)$$

C. Application of the inference scheme to a simulated population of BBH

We apply the above scheme to a simulated set of 1024 BBH GW events detected in LIGO and Virgo data assuming current sensitivities comparable to the recent O2 and O3 observing runs [9, 10, 52, 53] having detected BBH binaries between $3 M_{\odot}$ and $100 M_{\odot}$ up to redshift 1.5. Our synthetic catalog is thus compatible with the GWTC-1 and GWTC-2 catalogs [2, 27]. We choose a uniform in comoving volume merger rate $\gamma = 0$. We draw the BBH component masses in the source frame from the PL distribution defined by the two mass scales $m_{\text{min}} = 5 M_{\odot}$ and $m_{\text{max}} = 65 M_{\odot}$, and two parameters $\alpha = 0$ and $\beta = 0$ that governs the shape of the mass distribution. The simulated events pass the detection criterion that requires an SNR of at least 12 [25]. We fix a flat Λ CDM cosmology with $H_0 = 67.7 \text{ km Mpc}^{-1} \text{ s}^{-1}$ and $\Omega_{m,0} = 0.308$ [54]. In this section and Sec. IV uncertainties on the measurements of the source-frame masses are generated with the likelihood approximant of [43], while redshift uncertainties are generated with the likelihood approximant of [55].

We consider the case in which $\Omega_{m,0}$ is fixed to the Planck value, namely $\Omega_{m,0} = 0.308$ [54], and a second case where $\Omega_{m,0}$ is able to vary in the range $[0.1, 0.9]$ with a uniform prior. In both cases, we estimate mass model parameters and the rate evolution jointly with H_0 and $\Omega_{m,0}$ if it is left free.

Fig. 1 shows the marginal posterior distributions that we obtain as we collect more GW events. In the next section we further discuss the results of this simulation.

III. EFFECT OF COSMOLOGICAL AND SOURCE POPULATION HYPERPARAMETERS

Previous works such as [38, 39, 43–45] have already discussed the possibility of constraining cosmology by exploiting features in the source-frame mass spectrum (such

as cut-offs or peaks). In the following, we estimate the impact of the population parameters — particularly $\Omega_{m,0}$ and m_{max} — on cosmological inference. We then discuss the achieved accuracy on cosmological parameters as a function of the size of the number of detected events.

A. Impact of $\Omega_{m,0}$

We find that $\Omega_{m,0}$ does not strongly impact the estimation of the mass-related population parameters, though it has a non-negligible impact on the estimation of H_0 . In the specific case of our simulations, based on current detector sensitivities, the impact of $\Omega_{m,0}$ is observed above ~ 200 detected events. In general, however, this number of events depends on the GW likelihood model used to simulate redshift and mass uncertainties for individual events. A fairly robust rule of thumb is that when the H_0 accuracy is about 40%, $\Omega_{m,0}$ starts to matter (see also Fig. 1).

With 1000 GW detections, we estimate H_0 with a 10% accuracy when fixing $\Omega_{m,0}$ to the true value, while this accuracy falls to 20% if we leave $\Omega_{m,0}$ to vary. This results from the strong correlation between $\Omega_{m,0}$ and H_0 for the determination of the GW luminosity distance as shown in Fig. 2, in which we plot the marginal posterior distributions obtained with 1024 BBH events.

While $\Omega_{m,0}$ cannot be measured with thousands of GW detections, this parameter has a clear impact on the H_0 determination. With the current number of GW detections and sensitivities, one can neglect the uncertainties on $\Omega_{m,0}$, but this should be reconsidered when analysing more GW events, especially if they are at higher redshifts. This last comment is consistent with the conclusion of [44] for third generation detectors.

B. Impact of the upper bound m_{max} of the mass spectrum

Concerning the component mass spectrum, we find that the most important parameter for the H_0 measurement is the maximum production mass m_{max} of BBHs. (This was already recognized by [43].) Fig. 3 shows the joint (H_0, m_{max}) posterior distribution when $\Omega_{m,0}$ is fixed, obtained with 32 GW events. There is a strong correlation between the determination of H_0 and m_{max} .

In fact the determination of m_{max} impacts the estimation of the H_0 in two ways. First, lower H_0 values drag the observed GW source to lower redshifts, which in turn leads to higher source-frame masses. This pushes the estimated masses toward the upper bound m_{max} . Some of the events may require their masses to exceed the bound and thus become incompatible with the model. Therefore low m_{max} are incompatible to small H_0 values.

Second, m_{max} also governs the fraction of events that we expect to detect at higher masses. A lack of detected sources with masses close to the expected m_{max} bound

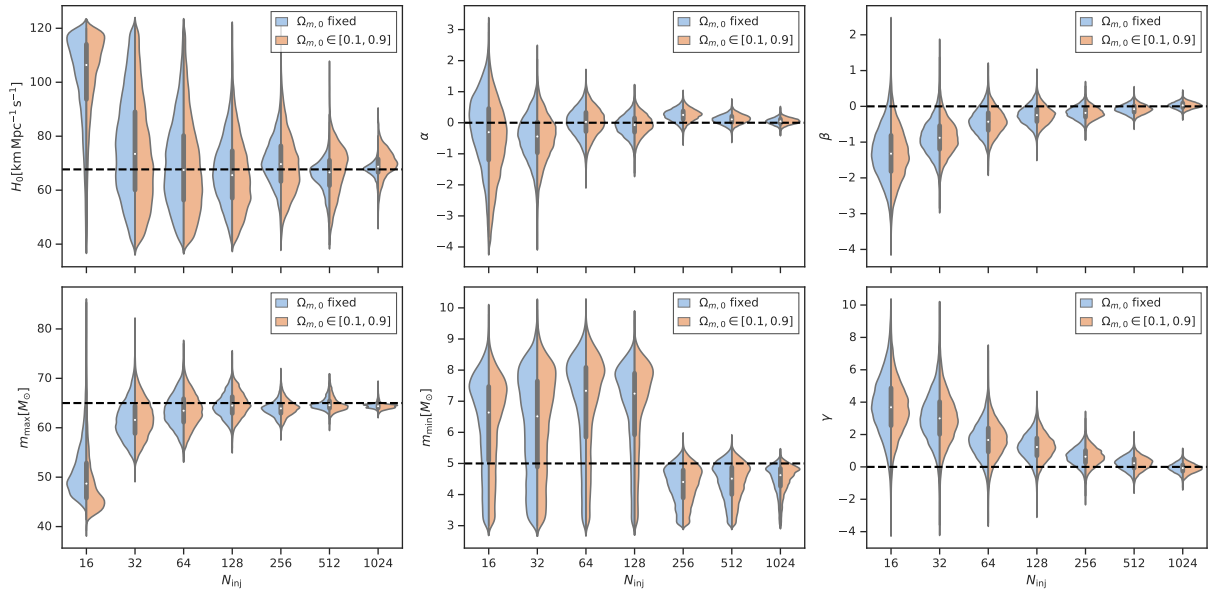


FIG. 1. Posterior probability density distributions on the different population parameters (PL mass model) as more and more GW detections are analyzed (horizontal axis). The horizontal black dashed line indicates the true parameters of the population. The blue posteriors are obtained by fixing $\Omega_{m,0} = 0.308$, while the orange posteriors are marginalized over the estimation of $\Omega_{m,0}$.

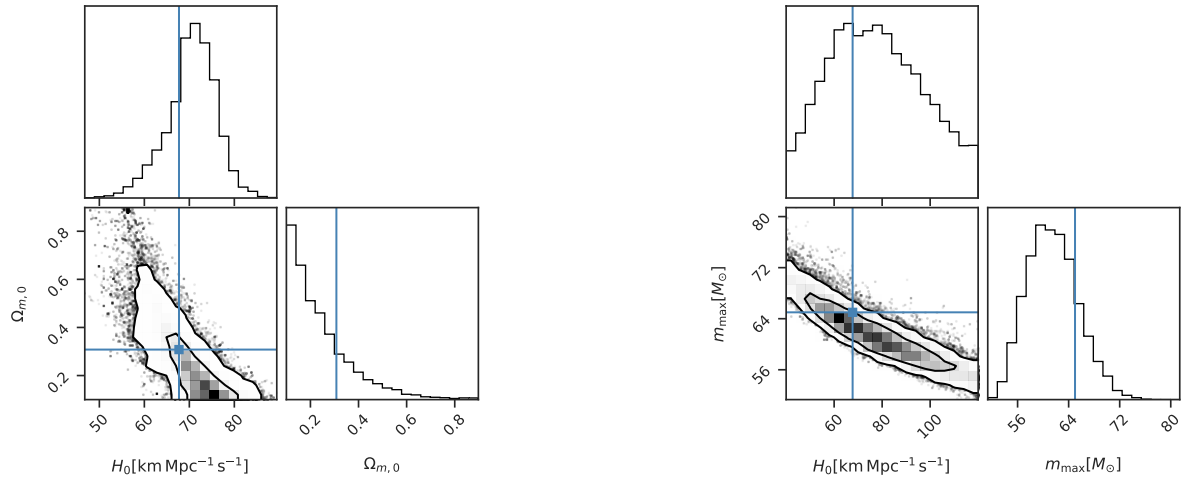


FIG. 2. Posterior distribution on the H_0 and $\Omega_{m,0}$ for 1024 BBH events detected with LIGO and Virgo at current sensitivities. The blue lines show the true parameters.

can be compensated by lowering m_{\max} or by increasing H_0 .

These two cross-correlations are clearly shown in Fig. 3 for 32 GW events. We see that this correlation plays an important role even when few events are observed.

While other parameters such as the rate evolution parameter, might cause a bias as demonstrated in the case of the Einstein Telescope by [44], for current sen-

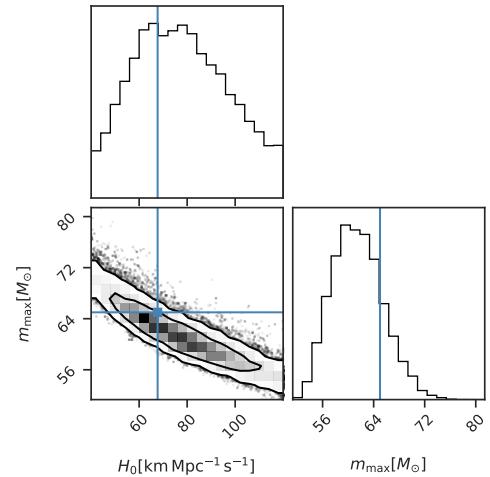


FIG. 3. Posterior distribution on the H_0 and m_{\max} for 32 BBH events detected with LIGO and Virgo at current sensitivities. The blue lines show the true parameters. In this case we fix $\Omega_{m,0} = 0.308$. The contours indicate the 1σ and 2σ confidence level intervals.

sitivities the m_{\max} parameter (or any other equivalent parametrization of a sharp break in the upper mass spectrum) thus appears crucial for the inference of the cosmological parameters.

C. Behaviour in the small and large sample regimes

The Bernstein-von Mises theorem (see e.g., [56]) states that, under mild assumptions (on the smoothness and continuity of the likelihood and prior distribution) and in the limit of large sample, the posterior distribution tends to a normal distribution centered at the maximum likelihood estimate with standard deviation $\propto 1/\sqrt{n}$. In this section we study the transition to this asymptotic behaviour and investigate the effect of model dimensionality.

1. Asymptotic normality and $1/\sqrt{n}$ error decay for large samples

From Fig. 1 we observe that the asymptotic regime is qualitatively reached when $N_{inj} \gtrsim 200$ for most of the parameters (with the exception of m_{min} whose distribution remains skewed for large samples). Fig. 6 confirms this findings and shows a $1/\sqrt{n}$ error decay for all parameters in the limit of large N_{inj} .

2. Discussion of the asymptotic accuracy for large samples

From Fig. 1 we conclude that m_{max} and H_0 (when fixing $\Omega_{m,0}$) are the two parameters that can be measured with the best accuracy, respectively at the 3% and 10% level (and 20% if $\Omega_{m,0}$ is left free). The other population parameters can be measured within 30% to 40% accuracy with $\gtrsim 1000$ signals. The rate evolution is the most difficult parameter to measure as we are looking at events at low redshift with current sensitivities.

We now compare the results above to the 5-year results presented in [43]. We obtain a similar accuracy for the estimation of H_0 alone (note that [43] measures $H(z=0.8)$ instead of H_0). In [43] the PISN mass scale is estimated with a greater precision up to $\sim 2\%$ in 5 years. There are, however, differences in the mass model. Instead of the smooth population decay above m_{max} assumed in [43], we consider a sharp cutoff. Compared to BNS-based measurements [38], our measurement uncertainty is smaller by a factor of ~ 5 .

The predictions made here are based on specific values for the population parameters. A larger positive value for α makes heavier BBH events rarer and harder to detect, thus decreasing the accuracy of the m_{max} estimate and pushing the transition to the asymptotic regime to larger N_{inj} .

3. Inconsistency in the small sample regime

We now elaborate on the estimation consistency (i.e., compatibility of the posterior with the true parameter value) for small sample sizes. When the number of events is $\lesssim 100$ the hierarchical inference is prone to statistical

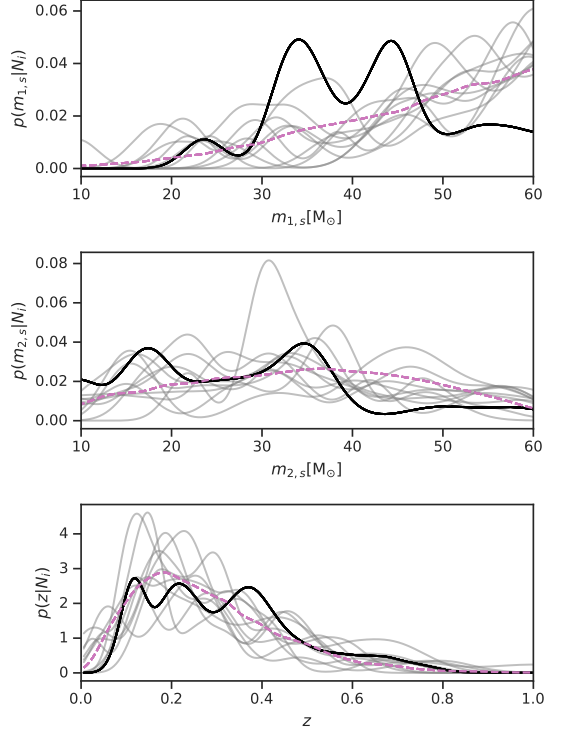


FIG. 4. Density of source-frame masses and cosmological redshift detected for 16 GW events (black) and expected (pink dashed line). The source-frame quantities are calculated assuming a population-induced prior fixed to the one with the true population parameters. The gray shaded lines shows the distributions of another 50 independent sub-populations of 16 events.

fluctuations associated with specific population realizations. In Fig. 1 the true values appear only “weakly” or “broadly” compatible with the posterior envelope when $N_{inj} \lesssim 100$.

The results of the hierarchical inference scheme should thus be treated with caution when using a small sample. As an example, we select a sub-sample of 16 detected GW injections from the data set used in Fig. 1. In Fig. 4 we show the distributions of redshift and source-frame masses obtained with this small sample compared to the expected distribution and several realizations of 16 events sub-populations. Redshift uncertainties are accounted for and population-induced priors are fixed to injected population priors. The detected distribution does not match the expected distribution, especially for the mass parameters.

This disagreement induces cascading effects on the estimation of all population parameters. In Fig. 1 the inferred m_{max} value for $N_{inj} = 16$ appears to be underestimated thus leading to higher values for H_0 as this range of value is compatible with a population of lower source-frame mass sources placed at higher redshifts.

Interestingly, the presence of statistical effects due to small sample sizes are difficult to diagnose with stan-

dard sanity checks usually used in Bayesian analyses. Fig. 5 displays the so-called posterior predictive check conditioned on the GW detections. This check consists in overlapping the *expected* distribution of GW detections, obtained using the estimated population parameters, namely:

$$p_{\text{pop}}(\theta|\{x\}, N_{\text{obs}}) = \int p_{\text{det}}(\theta, \Lambda) \times p_{\text{pop}}(\theta|\Lambda)p(\Lambda|\{x\}, N_{\text{obs}}) d\Lambda \quad (9)$$

with the distribution of *detected* events (using population-induced priors). If the model is correct, the two cumulative distributions agree and the sanity check is passed.

This is what we observe in Fig. 5 where the posterior sanity check is computed for a small sample set with $N_{\text{inj}} = 16$. In this situation we would conclude that the fitted PL model agrees with the data and the population and cosmology parameters are thus reliably estimated. However this is misleading as those parameters are marginally compatible with the true value as indicated in Fig. 1.

Such sanity check verifies the ability of the population model to capture the features of the observed population but it does not provide information about the reliability of the cosmological parameter estimates. Drawing conclusions on population parameters from single (or exceptional events) should thus be done carefully if the analysis does not take into account in any form previous detections.

IV. IMPACT OF POPULATION MISCALIBRATION

In this section we discuss the systematics on the estimation of H_0 due to population miscalibration. Here, we fix $\Omega_{m,0}$ to the true value although, as shown in Sec. III A this parameter is also impacted.

A. Choosing the wrong mass upper-bound m_{max}

We have seen in Sec. III B that the parameter m_{max} (or any other parameters related to features in the source-frame mass spectrum) plays a fundamental role for the inference of H_0 . A prior for m_{max} has to be chosen *a priori*. The choice of a particular value can be motivated by physical arguments related to theories of BH formation, e.g., such as the existence of the PISN in a narrow mass region [42]) or by heuristic arguments in order to accommodate a specific observation, e.g., as in the case of GW190521 [16, 17]. In this section we discuss the consequence of fixing m_{max} to a value inconsistent with the true value.

Fig. 7 shows the posterior distribution obtained for the population parameters when fixing the $m_{\text{max}} = 85M_{\odot}$ when the true value used in the simulation is $m_{\text{max}} =$

$65M_{\odot}$. In this case we thus fix the maximum mass to a value *higher* than the true value. The expectation is that the inferred source population parameters will be fitted so that the distribution of detected events matches the incorrect upper bound at $m_{\text{max}} = 85M_{\odot}$, while the other hyperparameters will be tuned in order to reduce the lack of events observed in the range from 65 to $85M_{\odot}$. Thus we expect a systematic bias.

We observe in Fig. 7 that H_0 is biased towards smaller values and the GW events estimated at lower redshifts with higher source-frame masses. Also, the rate evolution parameter converges to negative values in order to prefer events that are at lower redshifts in order to obtain a population of events with higher source-frame masses. In this particular case, the PL slope is also biased to favour the excess lower mass events.

Choosing the wrong maximum mass has an impact on H_0 with the current number of observed events in the GWTC1 and GWTC2 catalogs, as shown in Fig. 8 obtained with 64 GW signals.

Conversely to above, when m_{max} is set to a *lower* value than the true value, H_0 is biased towards higher values. The inference of the lower mass gap and the parameters β , related to the PL slope of the second mass are mostly unaffected by the choice of m_{max} .

In summary fixing the maximum mass for BH production can thus lead to biased estimations of the cosmological and source population parameters and in particular of H_0 .

B. Using an incomplete model

We now discuss the impact of selecting an incomplete population model that misses some of the features of the more complex mass spectrum in force. To this aim, we simulate a population of BBHs using a PLG model for the source-frame mass spectrum and assuming a flat Λ CDM cosmology with $H_0 = 67.7 \text{ km Mpc}^{-1} \text{ s}^{-1}$.

The Gaussian component of the primary mass spectrum has $\mu_g = 40M_{\odot}$ and $\sigma_g = 5M_{\odot}$. The fraction of the Gaussian component relative to the PL component is $\lambda_g = 10\%$. The PL component has $m_{\text{min}} = 5M_{\odot}$, $m_{\text{max}} = 75M_{\odot}$, $\alpha = 2$ and $\beta = 1$. A tapering factor of $\delta_m = 3M_{\odot}$ is applied to the lower mass cut-off.

Fig. 9 shows the discrepancy in terms of number of σ between the estimated and true values of the parameters. For low numbers of GW detections (low-sample regime) this figure of merit may not be very robust as posteriors may have tails. However, for large number of events the posteriors “gaussianize”, we should find the true values in a reasonable confidence interval, say within 2.5σ .

Using the correct PL model to fit the population, we obtain that for any number of detected GW signals, the true population parameters are within the 2.5σ confidence levels.

Instead, when using the PL model to fit the more complex PLG model, the estimations of m_{min} and H_0 depart

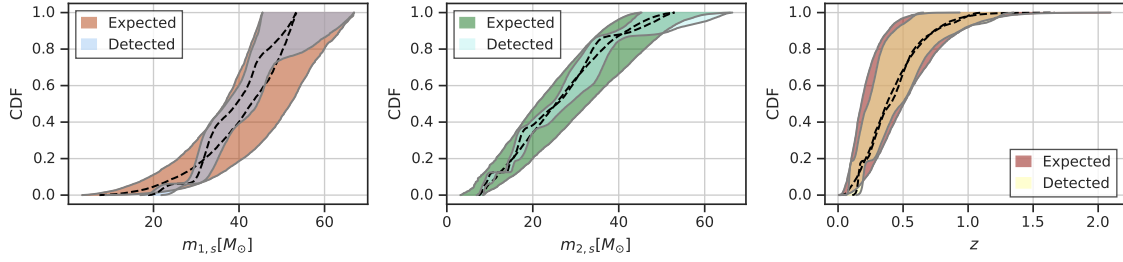


FIG. 5. Posterior predictive check for the source-frame masses and cosmological redshift. The shaded area correspond to the 90% confidence level calculated from the population parameters posterior for the 16 events analyzed in II. The black dashed line indicates the median (or the 50% percentile) for the posterior predictive check.

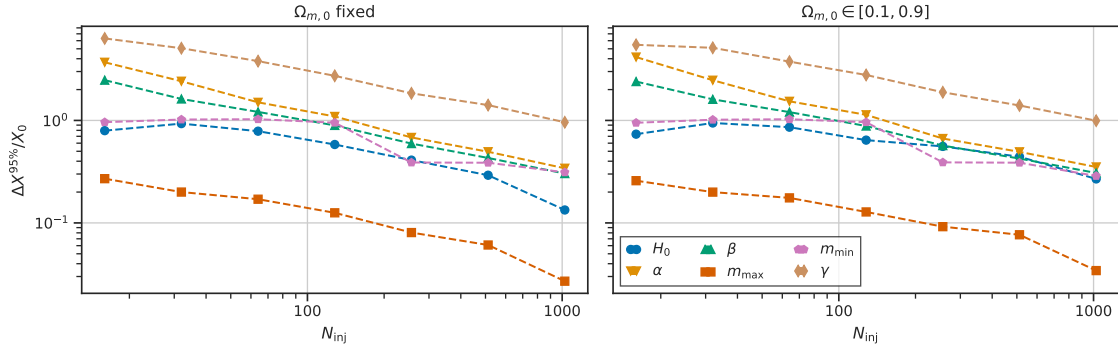


FIG. 6. *Left:* Fractional error at 90% confidence level for the population parameters. $\Omega_{m,0}$ is fixed to its true value. *Right:* Same as the left plot but leaving $\Omega_{m,0}$ to vary.

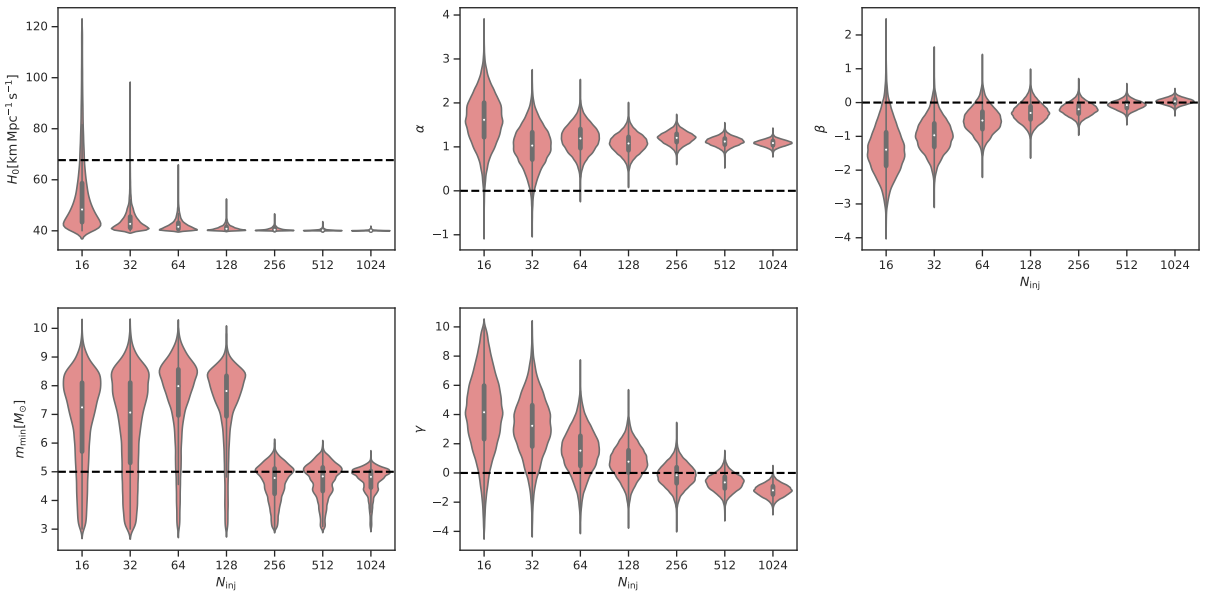


FIG. 7. Posterior envelope for several population parameters obtained fixing $m_{\text{max}} = 85 M_{\odot}$ and varying the number of GW detections analysed. The larger the number of GW detections, the larger the bias introduced by the wrong choice of m_{max} . The black dashed line indicates the true value.

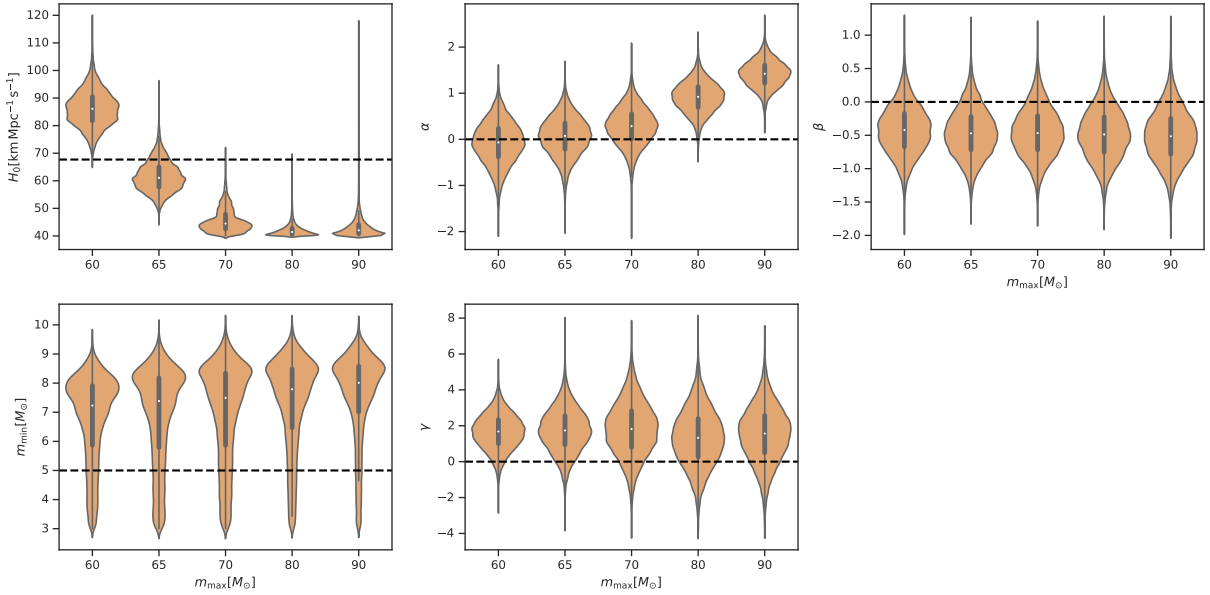


FIG. 8. This figures show the posterior envelope for several population parameters obtained fixing the number of GW events analyzed to 64 but varying m_{\max} . The black dashed line indicate the injected value. The true value of m_{\max} is $65 M_{\odot}$.

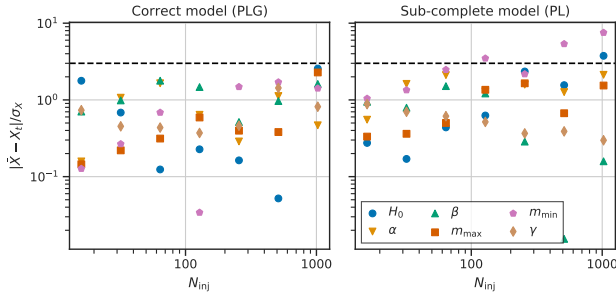


FIG. 9. Discrepancy in terms of σ between the estimated and true value of parameter X (where X is any of the parameters listed in the legend). The dashed horizontal line indicates the 3σ confidence level. The true population model is PLG. *Left plot*: Fit the correct model (PLG) ($\Omega_{m,0}$ fixed). *Right plot*: Fit of an incorrect and incomplete model (PL).

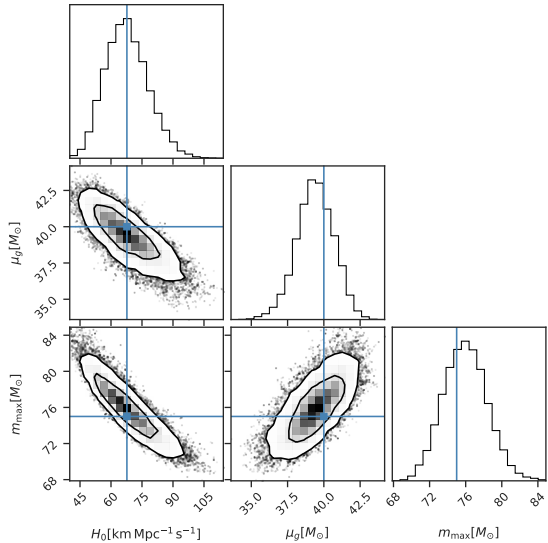


FIG. 10. Posterior probability density for μ_g, m_{\max} and H_0 for 512 GW injections. The blue lines identify the true parameters of the simulation.

from the true values by more than 6 and 3σ respectively.

The reason for failing to estimate m_{\min} correctly is the lack of tapering at low masses for the PL model, while the issue with H_0 is the impossibility for the PL model to fit the events from the Gaussian peak of the PLG model.

The determination of the Gaussian peak has a prevalent role in fitting the cosmological parameters. Fig. 10 shows the marginal posterior distributions for m_{\max} , μ_g and H_0 for the PLG model. As explained above, since μ_g governs a sharp feature in the mass spectrum, it correlates with the determination of H_0 and m_{\max} .

In conclusion, (over)simplified population models must be handled with care as that may lead to significant bias when the true mass spectrum has a complex shape. It is therefore essential to make a thorough goodness-of-fit

evaluation of several models using Bayes factor. In the above example this would have shown that PLG was the preferred model.

V. THE IMPACT OF POPULATION ASSUMPTIONS FOR O2 COSMOLOGY AND FUTURE FORECASTS

In this section, we provide further evidence of the important role played by population assumptions in cosmological inference in the context of two practical cases with relevance to current and future GW data sets.

We first re-examine the estimation of H_0 obtained with GWTC-1 in [25] in light of the above observations.

Second, we present results of a joint cosmological and source population inference using the expected sensitivity for the future observing run O4. This study is produced directly from (simulated) GW $h(t)$ data and are based on posterior samples generated from Bayesian samplers used for GW parameter estimation. This thus reproduces the “end-to-end” analysis chain from observational data.

A. Re-estimation of H_0 based on the O2/GWTC-1 catalog

The analysis in [25] is based on the “brightest” BBHs of the GWTC-1 catalog selected with $\text{SNR} > 12$ (6 events in total). The H_0 measurement uses redshift information from the GLADE [57] and DES [58] galaxy catalogs. Out of the six considered BBHs events, two have a low probability for their hosting galaxy to be in the galaxy catalogs (GW170104 and GW170809), three have a medium probability (GW150914, GW151226 and GW170608), while one has a probability almost equal to 1 (GW170814).

The analysis in [25] *a priori* assumes a source population based on the PL model. The reference analysis in [25] based on gwcsmo [59] fixes these parameters to $\Lambda_m = \{m_{\max} = 100 M_\odot, m_{\min} = 5 M_\odot, \alpha = 1.6, \beta = 0\}$. These values were chosen to accommodate all possible values for the source-frame masses of the GW events in the GWTC-1 and GWTC-2 catalogs for any choice of $H_0 \in [20, 140] \text{ km Mpc}^{-1} \text{ s}^{-1}$. Based on those assumptions the analysis draw samples from the posterior

$$p(H_0 | \Lambda_m, x) = p(x | H_0, \Lambda_m) p(H_0). \quad (10)$$

In light of the results presented above, we anticipate that those assumptions will impact on the accuracy and uncertainty of final H_0 estimate. [25] partially addresses this issue and discusses possible systematics due to the uncertainty on the m_{\max} and α parameters.

We investigate this question by repeating the analysis of [25], with a different prior determination of the source population parameters obtained by first applying the inference scheme introduced in Sec. II. This initial step does not rely on galaxy catalogs, and is thus

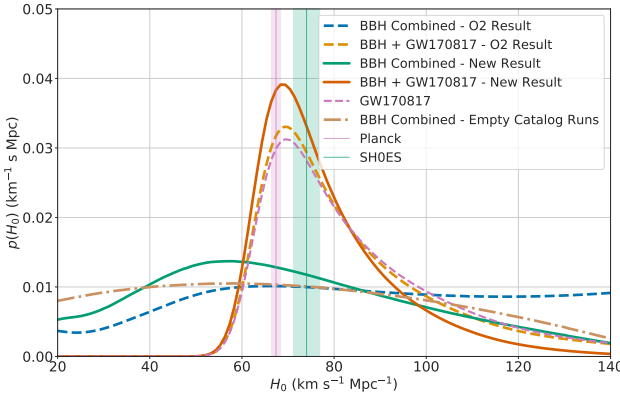


FIG. 11. Posterior distribution on H_0 using the 6 GWTC-1 events with $\text{SNR} > 12$ and the GLADE and DES galaxy catalogs. The plot compares the results obtained in [25] with the new results of this paper (see discussion in Sec. V A).

similar in essence to an analysis that would use incomplete galaxy catalogs. In a sense, this provides an initial “calibration” of the source population parameters with an agnostic analysis.

We run the joint population and cosmology analysis using the same set of GWTC-1 BBH events. We fix β and $\gamma = 0$ and allow m_{\min} , m_{\max} and α to vary. We specifically target the region associated with the current tension on the H_0 estimate, and use for H_0 a uniform prior in the range [67, 74] $\text{km Mpc}^{-1} \text{s}^{-1}$. With these settings, the maximum likelihood is reached at $H_0 = 69 \text{ km Mpc}^{-1} \text{s}^{-1}$ with the parameters $m_{\min} = 8.6 M_{\odot}$, $m_{\max} = 37.5 M_{\odot}$ and $\alpha = 2.2$. Those parameters best fit the data in the region of interest for H_0 but may not for other values.

In a second step we apply the analysis of [25] using the GLADE and DES galaxy catalogs using the new set of population parameters. Fig. 11 shows the results for both approaches. We obtain the credible interval $H_0 = 68^{+13}_{-7} \text{ km Mpc}^{-1} \text{s}^{-1}$ to be compared to $H_0 = 68^{+16}_{-8} \text{ km Mpc}^{-1} \text{s}^{-1}$ reported in [25]. The width of the former is about 15% narrower; the H_0 estimate is thus more informative in the tension region.

In Fig. 11 the posterior tails appear considerably reduced with the new choice of population parameters; not surprisingly, as those parameters maximize the likelihood in the central H_0 -tension region.

This case study shows population assumptions matter as they impact on the final measurement accuracy. In the absence of a strong prior belief for the population model, this advocates for analysis schemes that *consider population and cosmological parameters jointly* and not separately. This suggests to perform joint source population and cosmological inference together with the use of galaxy catalogs. Combining the two analyses is not obvious and likely leads to challenging computational issues. If this turns out to be intractable, a comprehensive evaluation of the systematics induced by population assumptions are required to deduce robust conclusions from

analyses that treat source population and cosmology separately.

B. End-to-end analysis from GW data

For convenience the results presented in Sec. III and IV are based on an approximated likelihood [43] that allows generating posterior distributions over large numbers of GW events. In this section we validate our results by an “end-to-end” analysis that uses the exact likelihood and infer posterior distributions starting from GW $h(t)$ data.

We simulate a mock BBH catalog and generate the associated GW signals using the `IMRPhenomD` [60] waveform approximant. We retain 100,000 signals detected with a minimum SNR of 12 by the LIGO-Virgo three-detector network at design sensitivities ¹.

From this catalog we select 200 events in such a way that they mimic a population with a PL mass distribution with parameters $\alpha = 2$, $\beta = 0$, $m_{\min} = 35 M_{\odot}$ and $m_{\max} = 65 M_{\odot}$. The choice for m_{\min} is not representative of realistic astrophysical expectations. It is made to speed up the analysis as it avoids the Bayesian estimation of low-mass events which takes substantially more time.

We furthermore assume that the sources are distributed uniformly in comoving volume with a rate evolving parameter $\gamma = 2$, in a range of 100 Mpc to 13 Gpc. The spins are assumed aligned with the orbital momentum.

The selected subset of 200 events is processed by the inference pipeline `Bilby` using the Bayesian sampler `dynesty` [61]. We run a full 10-dimensional parameter estimation (since we fix the coalescence time of the merger and assume aligned spins). We assume standard priors on the spin amplitudes, the polarization angle, sky position, inspiral phase, a d_L^2 prior on luminosity distance (which is later removed in the population analysis) and flat priors on the detector frame masses. For this latter sampling we do not impose the $m_{2,d} < m_{1,d}$ condition on the component masses, but apply it *a posteriori*.

We first compare the posteriors obtained from the full parameter estimation with those obtained with the approximation [43] used in Sec. II. Figs. 12 and 13 show two illustrative events. The first has a network SNR $\rho = 38$ well above the detection threshold and the second has a network SNR $\rho = 13$ closer to the detectability limit. For completeness, we provide the other parameters in the figure captions.

The posterior distribution based on the approximated likelihood (in black) strongly underestimates the uncertainties for all parameters, and does not capture the correlation between the detector frame masses and the luminosity distance. We thus conclude that the uncertainties

¹ <https://dcc.ligo.org/LIGO-T2000012/public>

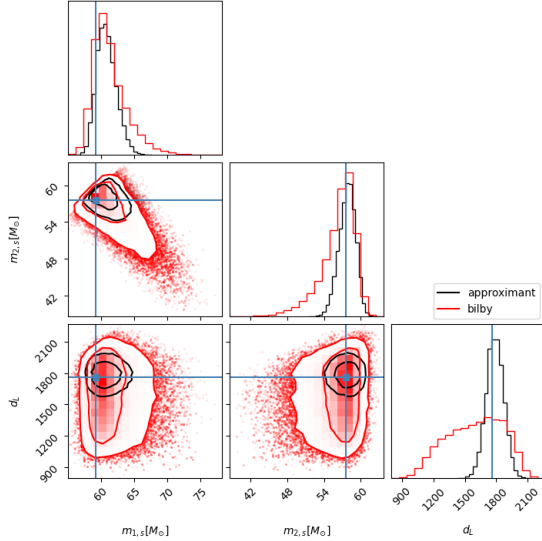


FIG. 12. Posterior distributions for the detector frame masses and luminosity distance obtained from an end-to-end Bayesian inference using Bilby (in red) and the approximated likelihood [43] (in black). The event is observed with a network SNR of 38. The source frame masses are $m_{1,s} = 44.6 M_{\odot}$ and $m_{2,s} = 43.5 M_{\odot}$ while the binary inclination angle is $\iota \sim 149$ deg. The true parameters are indicated with blue lines.

given in Sec. II are optimistic estimates compared to a realistic end-to-end analysis.

We then perform the analysis outlined in Sec. II to estimate the population parameters, jointly with H_0 . Fig. 14 shows the marginal posterior distributions obtained with the 200 selected events.

The posterior distributions for the cosmological and population parameters are in good agreement with the true value. This thus provides a proof-of-principle for the applicability of the approach to real data.

Though hundreds of events with non-Gaussian individual posteriors are combined, the posterior distributions converge to a normal distribution as noted in Sec III C 1.

We notice a significant correlation between the lower-mass limit m_{\min} and H_0 , that was not present in the earlier simulations. This is a consequence of the higher value for m_{\min} used for this simulation. A much larger number of events is now informative on the lower mass cut-off of the mass spectrum, which can thus be accurately measured. Together with m_{\max} the measurement of m_{\min} provides an additional well-defined mass scale that correlates with H_0 . This does not impact on the final accuracy level of the H_0 measurement which appears the same as in the case where $m_{\min} = 5 M_{\odot}$.

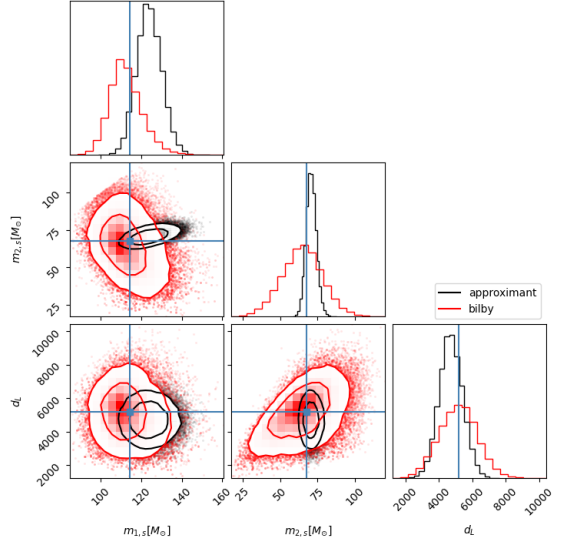


FIG. 13. Posterior distributions for the detector frame masses and luminosity distance obtained from an end-to-end Bayesian inference using Bilby (in red) and the approximated likelihood [43] (in black). The event is observed with a network SNR of 13. The source frame masses are $m_{1,s} = 63.6 M_{\odot}$ and $m_{2,s} = 37.6 M_{\odot}$ while the binary inclination angle is $\iota \sim 157$ deg.

VI. CONCLUSIONS

In this paper we discussed the impact of population assumptions for cosmological inference with GW events. We showed that, even with current sensitivities, population assumptions on the feature of the mass spectrum can affect the estimation of the cosmological parameters H_0 and $\Omega_{m,0}$.

We found that the parameters that governs the position of the middle peak or of high-mass cut-off in the mass spectrum are strongly correlated with the final estimated value for H_0 . We also showed that incorrect priors about the properties of those features introduce a significant bias.

Together with the uncertainties of GW data calibration [62] and the misevaluation of selection effects due to the BNS viewing angle [63], population assumptions could represent the major and possibly dominant source of systematics for GW-based cosmology with current and future GW observations.

That is why we argue that cosmological and population parameters should be performed jointly. However, this can be computationally challenging given the large number of galaxies that has to be considered and the rapidly increasing number of GW detections. Those computational challenges can possibly be resolved by porting the inference code to GPU [64].

It is necessary that GW-based cosmological analysis is complemented with a comprehensive and in-depth eval-

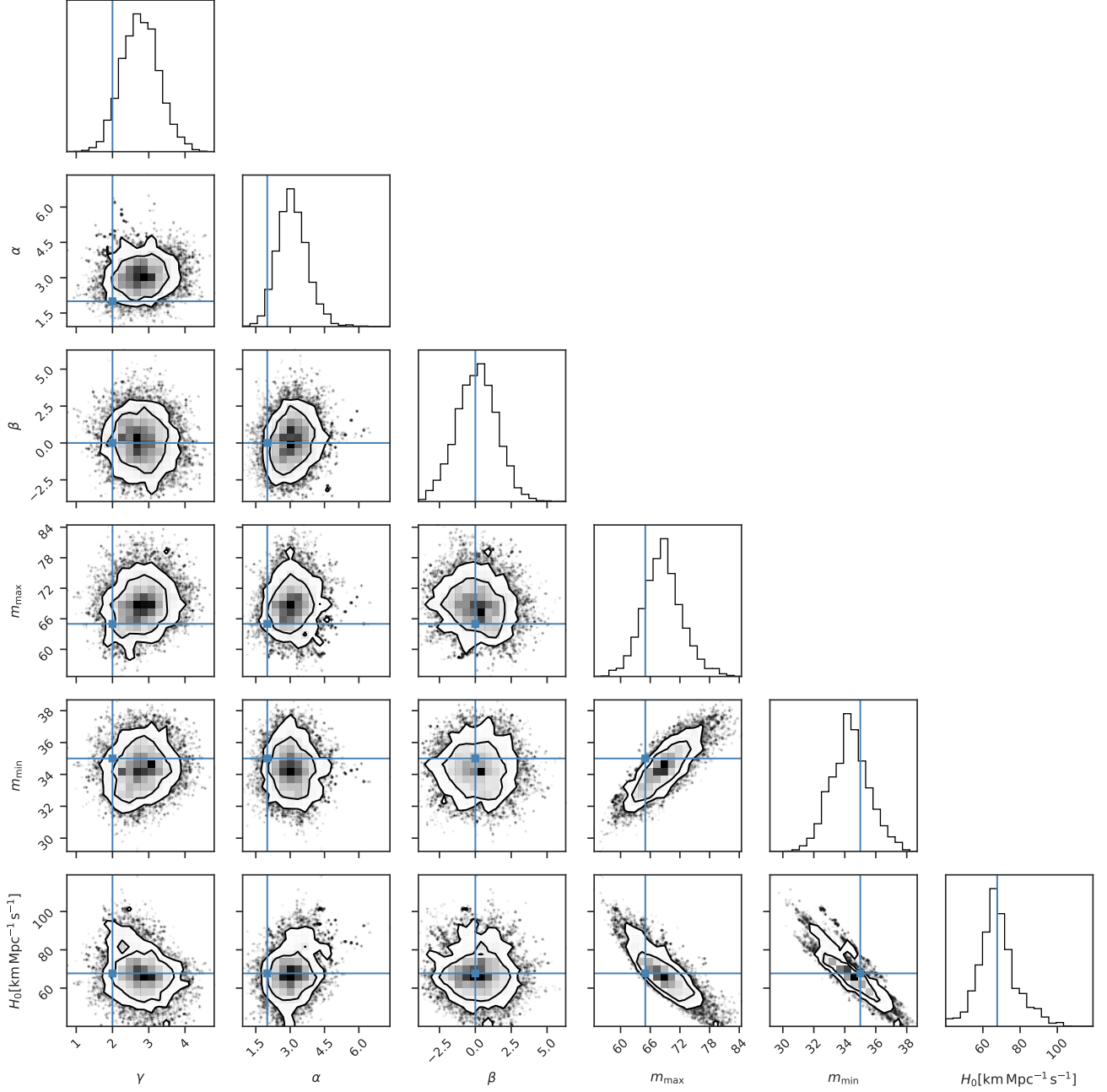


FIG. 14. Posterior probability density distributions for the population parameters and the H_0 using posterior from 200 events generated with full parameter estimation. The blue lines indicate the population injected values. Levels indicate the 68% and 90% confidence intervals.

uation of the impact of population assumptions on the final result.

ACKNOWLEDGMENT

SM is supported by the LabEx UnivEarthS (ANR-10-LABX-0023 and ANR-18-IDEX-0001), of the European Gravitational Observatory and of the Paris Center

for Cosmological Physics. KL is grateful to the Fondation CFM pour la Recherche in France for supporting his PhD. The authors are grateful for computational resources provided by the LIGO Laboratory and supported by National Science Foundation Grants PHY-0757058 and PHY-0823459. CK is partially supported by the Spanish MINECO under the grants SEV-2016-0588 and PGC2018-101858-B-I00, some of which include ERDF funds from the European Union. IFAE is partially funded

by the CERCA program of the Generalitat de Catalunya.
RG is supported by the Science and Technology Facilities
Council.

[1] **LIGO Scientific, Virgo** Collaboration, B. P. Abbott *et al.*, “Observation of Gravitational Waves from a Binary Black Hole Merger,” *Phys. Rev. Lett.* **116** no. 6, (2016) 061102, [arXiv:1602.03837 \[gr-qc\]](https://arxiv.org/abs/1602.03837).

[2] **LIGO Scientific, Virgo** Collaboration, B. P. Abbott *et al.*, “GWTC-1: A Gravitational-Wave Transient Catalog of Compact Binary Mergers Observed by LIGO and Virgo during the First and Second Observing Runs,” *Phys. Rev. X* **9** no. 3, (2019) 031040, [arXiv:1811.12907 \[astro-ph.HE\]](https://arxiv.org/abs/1811.12907).

[3] B. S. Sathyaprakash and B. F. Schutz, “Physics, Astrophysics and Cosmology with Gravitational Waves,” *Living Rev. Rel.* **12** (2009) 2, [arXiv:0903.0338 \[gr-qc\]](https://arxiv.org/abs/0903.0338).

[4] D. E. Holz and S. A. Hughes, “Using gravitational-wave standard sirens,” *Astrophys. J.* **629** (2005) 15–22, [arXiv:astro-ph/0504616](https://arxiv.org/abs/astro-ph/0504616).

[5] A. G. Riess *et al.*, “A 2.4% Determination of the Local Value of the Hubble Constant,” *Astrophys. J.* **826** no. 1, (2016) 56, [arXiv:1604.01424 \[astro-ph.CO\]](https://arxiv.org/abs/1604.01424).

[6] **Planck** Collaboration, N. Aghanim *et al.*, “Planck 2018 results. VI. Cosmological parameters,” *Astron. Astrophys.* **641** (2020) A6, [arXiv:1807.06209 \[astro-ph.CO\]](https://arxiv.org/abs/1807.06209).

[7] W. L. Freedman, “Cosmology at a Crossroads,” *Nature Astron.* **1** (2017) 0121, [arXiv:1706.02739 \[astro-ph.CO\]](https://arxiv.org/abs/1706.02739).

[8] A. G. Riess, S. Casertano, W. Yuan, L. M. Macri, and D. Scolnic, “Large Magellanic Cloud Cepheid Standards Provide a 1% Foundation for the Determination of the Hubble Constant and Stronger Evidence for Physics beyond Λ CDM,” *Astrophys. J.* **876** no. 1, (2019) 85, [arXiv:1903.07603 \[astro-ph.CO\]](https://arxiv.org/abs/1903.07603).

[9] **LIGO Scientific** Collaboration, J. Aasi *et al.*, “Advanced LIGO,” *Class. Quant. Grav.* **32** (2015) 074001, [arXiv:1411.4547 \[gr-qc\]](https://arxiv.org/abs/1411.4547).

[10] **VIRGO** Collaboration, F. Acernese *et al.*, “Advanced Virgo: a second-generation interferometric gravitational wave detector,” *Class. Quant. Grav.* **32** no. 2, (2015) 024001, [arXiv:1408.3978 \[gr-qc\]](https://arxiv.org/abs/1408.3978).

[11] B. F. Schutz, “Determining the Hubble constant from gravitational wave observations,” *Nature* **323** no. 6086, (Sept., 1986) 310–311.

[12] **LIGO Scientific, Virgo, 1M2H, Dark Energy Camera GW-E, DES, DLT40, Las Cumbres Observatory, VINROUGE, MASTER** Collaboration, B. P. Abbott *et al.*, “A gravitational-wave standard siren measurement of the Hubble constant,” *Nature* **551** no. 7678, (2017) 85–88, [arXiv:1710.05835 \[astro-ph.CO\]](https://arxiv.org/abs/1710.05835).

[13] **LIGO Scientific, Virgo** Collaboration, B. P. Abbott *et al.*, “Properties of the binary neutron star merger GW170817,” *Phys. Rev. X* **9** no. 1, (2019) 011001, [arXiv:1805.11579 \[gr-qc\]](https://arxiv.org/abs/1805.11579).

[14] **LIGO Scientific, Virgo** Collaboration, B. P. Abbott *et al.*, “GW170817: Observation of Gravitational Waves from a Binary Neutron Star Inspiral,” *Phys. Rev. Lett.* **119** no. 16, (2017) 161101, [arXiv:1710.05832 \[gr-qc\]](https://arxiv.org/abs/1710.05832).

[15] M. J. Graham *et al.*, “Candidate Electromagnetic Counterpart to the Binary Black Hole Merger Gravitational Wave Event S190521g,” *Phys. Rev. Lett.* **124** no. 25, (2020) 251102, [arXiv:2006.14122 \[astro-ph.HE\]](https://arxiv.org/abs/2006.14122).

[16] **LIGO Scientific, Virgo** Collaboration, R. Abbott *et al.*, “Properties and Astrophysical Implications of the $150 M_{\odot}$ Binary Black Hole Merger GW190521,” *Astrophys. J. Lett.* **900** no. 1, (2020) L13, [arXiv:2009.01190 \[astro-ph.HE\]](https://arxiv.org/abs/2009.01190).

[17] **LIGO Scientific, Virgo** Collaboration, R. Abbott *et al.*, “GW190521: A Binary Black Hole Merger with a Total Mass of $150 M_{\odot}$,” *Phys. Rev. Lett.* **125** no. 10, (2020) 101102, [arXiv:2009.01075 \[gr-qc\]](https://arxiv.org/abs/2009.01075).

[18] H.-Y. Chen, C.-J. Haster, S. Vitale, W. M. Farr, and M. Isi, “A Standard Siren Cosmological Measurement from the Potential GW190521 Electromagnetic Counterpart ZTF19abranhr,” [arXiv:2009.14057 \[astro-ph.CO\]](https://arxiv.org/abs/2009.14057).

[19] S. Mukherjee, A. Ghosh, M. J. Graham, C. Karathanasis, M. M. Kasliwal, I. Magaña Hernandez, S. M. Nissanke, A. Silvestri, and B. D. Wandelt, “First measurement of the Hubble parameter from bright binary black hole GW190521,” [arXiv:2009.14199 \[astro-ph.CO\]](https://arxiv.org/abs/2009.14199).

[20] S. Mastrogianni, D. A. Steer, and M. Barsuglia, “Probing modified gravity theories and cosmology using gravitational-waves and associated electromagnetic counterparts,” *Phys. Rev. D* **102** no. 4, (Aug., 2020) 044009, [arXiv:2004.01632 \[gr-qc\]](https://arxiv.org/abs/2004.01632).

[21] S. Mukherjee, G. Lavaux, F. R. Bouchet, J. Jasche, B. D. Wandelt, S. M. Nissanke, F. Leclercq, and K. Hotokezaka, “Velocity correction for Hubble constant measurements from standard sirens,” *Astron. Astrophys.* **646** (2021) A65, [arXiv:1909.08627 \[astro-ph.CO\]](https://arxiv.org/abs/1909.08627).

[22] C. Nicolaou, O. Lahav, P. Lemos, W. Hartley, and J. Braden, “The Impact of Peculiar Velocities on the Estimation of the Hubble Constant from Gravitational Wave Standard Sirens,” *Mon. Not. Roy. Astron. Soc.* **495** no. 1, (2020) 90–97, [arXiv:1909.09609 \[astro-ph.CO\]](https://arxiv.org/abs/1909.09609).

[23] **LIGO Scientific, Virgo** Collaboration, M. Fishbach *et al.*, “A Standard Siren Measurement of the Hubble Constant from GW170817 without the Electromagnetic Counterpart,” *Astrophys. J. Lett.* **871** no. 1, (2019) L13, [arXiv:1807.05667 \[astro-ph.CO\]](https://arxiv.org/abs/1807.05667).

[24] **DES, LIGO Scientific, Virgo** Collaboration, M. Soares-Santos *et al.*, “First Measurement of the Hubble Constant from a Dark Standard Siren using the Dark Energy Survey Galaxies and the LIGO/Virgo Binary-Black-hole Merger GW170814,” *Astrophys. J. Lett.* **876** no. 1, (2019) L7, [arXiv:1901.01540 \[astro-ph.CO\]](https://arxiv.org/abs/1901.01540).

[25] **LIGO Scientific, Virgo** Collaboration, B. P. Abbott *et al.*, “A Gravitational-wave Measurement of the Hubble Constant Following the Second Observing Run of Advanced LIGO and Virgo,” *Astrophys. J.* **909** no. 2, (2021) 218, [arXiv:1908.06060 \[astro-ph.CO\]](https://arxiv.org/abs/1908.06060).

[26] **LIGO Scientific, Virgo** Collaboration, R. Abbott *et al.*, “GW190814: Gravitational Waves from the Coalescence of a 23 Solar Mass Black Hole with a 2.6 Solar Mass Compact Object,” *Astrophys. J. Lett.* **896** no. 2, (2020) L44, [arXiv:2006.12611 \[astro-ph.HE\]](https://arxiv.org/abs/2006.12611).

[27] **LIGO Scientific, Virgo** Collaboration, R. Abbott *et al.*, “GWTC-2: Compact Binary Coalescences Observed by LIGO and Virgo During the First Half of the Third Observing Run,” [arXiv:2010.14527](https://arxiv.org/abs/2010.14527) [gr-qc].

[28] A. Finke, S. Foffa, F. Iacobelli, M. Maggiore, and M. Mancarella, “Cosmology with LIGO/Virgo dark sirens: Hubble parameter and modified gravitational wave propagation,” [arXiv:2101.12660](https://arxiv.org/abs/2101.12660) [astro-ph.CO].

[29] S. Mastrogiovanni, R. Duque, E. Chassande-Mottin, F. Daigne, and R. Mochkovitch, “What role will binary neutron star merger afterglows play in multimessenger cosmology?,” [arXiv:2012.12836](https://arxiv.org/abs/2012.12836) [astro-ph.HE].

[30] H.-Y. Chen, P. S. Cowperthwaite, B. D. Metzger, and E. Berger, “A Program for Multi-Messenger Standard Siren Cosmology in the Era of LIGO A+, Rubin Observatory, and Beyond,” [arXiv:2011.01211](https://arxiv.org/abs/2011.01211) [astro-ph.CO].

[31] M. Maggiore *et al.*, “Science Case for the Einstein Telescope,” *JCAP* **03** (2020) 050, [arXiv:1912.02622](https://arxiv.org/abs/1912.02622) [astro-ph.CO].

[32] M. Oguri, “Measuring the distance-redshift relation with the cross-correlation of gravitational wave standard sirens and galaxies,” *Phys. Rev. D* **93** no. 8, (2016) 083511, [arXiv:1603.02356](https://arxiv.org/abs/1603.02356) [astro-ph.CO].

[33] S. Mukherjee and B. D. Wandelt, “Beyond the classical distance-redshift test: cross-correlating redshift-free standard candles and sirens with redshift surveys,” [arXiv:1808.06615](https://arxiv.org/abs/1808.06615) [astro-ph.CO].

[34] S. Mukherjee, B. D. Wandelt, and J. Silk, “Probing the theory of gravity with gravitational lensing of gravitational waves and galaxy surveys,” *Mon. Not. Roy. Astron. Soc.* **494** no. 2, (2020) 1956–1970, [arXiv:1908.08951](https://arxiv.org/abs/1908.08951) [astro-ph.CO].

[35] S. Mukherjee, B. D. Wandelt, S. M. Nissanke, and A. Silvestri, “Accurate precision Cosmology with redshift unknown gravitational wave sources,” *Phys. Rev. D* **103** no. 4, (2021) 043520, [arXiv:2007.02943](https://arxiv.org/abs/2007.02943) [astro-ph.CO].

[36] S. Mukherjee, B. D. Wandelt, and J. Silk, “Testing the general theory of relativity using gravitational wave propagation from dark standard sirens,” [arXiv:2012.15316](https://arxiv.org/abs/2012.15316) [astro-ph.CO].

[37] D. Marković, “Possibility of determining cosmological parameters from measurements of gravitational waves emitted by coalescing, compact binaries,” *Phys. Rev. D* **48** (Nov, 1993) 4738–4756. <https://doi.org/10.1103/PhysRevD.48.4738>.

[38] S. R. Taylor, J. R. Gair, and I. Mandel, “Hubble without the Hubble: Cosmology using advanced gravitational-wave detectors alone,” *Phys. Rev. D* **85** (2012) 023535, [arXiv:1108.5161](https://arxiv.org/abs/1108.5161) [gr-qc].

[39] S. R. Taylor and J. R. Gair, “Cosmology with the lights off: standard sirens in the Einstein Telescope era,” *Phys. Rev. D* **86** (2012) 023502, [arXiv:1204.6739](https://arxiv.org/abs/1204.6739) [astro-ph.CO].

[40] B. Kiziltan, A. Kottas, M. De Yoreo, and S. E. Thorsett, “The Neutron Star Mass Distribution,” *ApJ* **778** no. 1, (Nov., 2013) 66, [arXiv:1011.4291](https://arxiv.org/abs/1011.4291) [astro-ph.GA].

[41] R. Valentim, E. Rangel, and J. E. Horvath, “On the mass distribution of neutron stars,” *Monthly Notices of the Royal Astronomical Society* **414** no. 2, (06, 2011) 1427–1431, <https://doi.org/10.1093/mnras/414/2/1427> [mnras/article-pdf/414/2/1427/30048].

[42] J. R. Bond, W. D. Arnett, and B. J. Carr, “The evolution and fate of Very Massive Objects,” *ApJ* **280** (May, 1984) 825–847.

[43] W. M. Farr, M. Fishbach, J. Ye, and D. Holz, “A Future Percent-Level Measurement of the Hubble Expansion at Redshift 0.8 With Advanced LIGO,” *Astrophys. J. Lett.* **883** no. 2, (2019) L42, [arXiv:1908.09084](https://arxiv.org/abs/1908.09084) [astro-ph.CO].

[44] Z.-Q. You, X.-J. Zhu, G. Ashton, E. Thrane, and Z.-H. Zhu, “Standard-siren cosmology using gravitational waves from binary black holes,” [arXiv:2004.00036](https://arxiv.org/abs/2004.00036) [astro-ph.CO].

[45] J. M. Ezquiaga and D. E. Holz, “Jumping the gap: searching for LIGO’s biggest black holes,” [arXiv:2006.02211](https://arxiv.org/abs/2006.02211) [astro-ph.HE].

[46] M. Fishbach, D. E. Holz, and W. M. Farr, “Does the Black Hole Merger Rate Evolve with Redshift?,” *Astrophys. J. Lett.* **863** no. 2, (2018) L41, [arXiv:1805.10270](https://arxiv.org/abs/1805.10270) [astro-ph.HE].

[47] **LIGO Scientific, Virgo** Collaboration, B. P. Abbott *et al.*, “Binary Black Hole Population Properties Inferred from the First and Second Observing Runs of Advanced LIGO and Advanced Virgo,” *Astrophys. J. Lett.* **882** no. 2, (2019) L24, [arXiv:1811.12940](https://arxiv.org/abs/1811.12940) [astro-ph.HE].

[48] **LIGO Scientific, Virgo** Collaboration, R. Abbott *et al.*, “Population Properties of Compact Objects from the Second LIGO-Virgo Gravitational-Wave Transient Catalog,” [arXiv:2010.14533](https://arxiv.org/abs/2010.14533) [astro-ph.HE].

[49] I. Mandel, W. M. Farr, and J. R. Gair, “Extracting distribution parameters from multiple uncertain observations with selection biases,” *Mon. Not. Roy. Astron. Soc.* **486** no. 1, (2019) 1086–1093, [arXiv:1809.02063](https://arxiv.org/abs/1809.02063) [physics.data-an].

[50] E. Thrane and C. Talbot, “An introduction to Bayesian inference in gravitational-wave astronomy: Parameter estimation, model selection, and hierarchical models,” *PASA* **36** (Mar., 2019) e010, [arXiv:1809.02293](https://arxiv.org/abs/1809.02293) [astro-ph.IM].

[51] S. Vitale, D. Gerosa, W. M. Farr, and S. R. Taylor, “Inferring the properties of a population of compact binaries in presence of selection effects,” [arXiv:2007.05579](https://arxiv.org/abs/2007.05579) [astro-ph.IM].

[52] **Virgo** Collaboration, F. Acernese *et al.*, “Increasing the Astrophysical Reach of the Advanced Virgo Detector via the Application of Squeezed Vacuum States of Light,” *Phys. Rev. Lett.* **123** no. 23, (2019) 231108.

[53] L. Instrument Science List, ;, A. Buikema, C. Cahillane, G. L. Mansell, C. D. Blair, R. Abbott, C. Adams, R. X. Adhikari, A. Ananyeva, and et al., “Sensitivity and Performance of the Advanced LIGO Detectors in the Third Observing Run,” *arXiv e-prints* (Aug., 2020) arXiv:2008.01301, [arXiv:2008.01301](https://arxiv.org/abs/2008.01301) [astro-ph.IM].

[54] **Planck** Collaboration, P. A. R. Ade *et al.*, “Planck 2015 results. XIII. Cosmological parameters,” *Astron. Astrophys.* **594** (2016) A13, [arXiv:1502.01589](https://arxiv.org/abs/1502.01589) [astro-ph.CO].

[55] M. Lagos, M. Fishbach, P. Landry, and D. E. Holz, “Standard sirens with a running Planck mass,” *Phys. Rev. D* **99** no. 8, (Apr., 2019) 083504, [arXiv:1901.03321](https://arxiv.org/abs/1901.03321) [astro-ph.CO].

[56] A. Van Der Vaart, *Asymptotic Statistics*. Cambridge Series in Statistical and Probabilistic Mathematics, 3. Cambridge University Press, 1998.

[57] G. Dálya, G. Galgócz, L. Dobos, Z. Frei, I. S. Heng, R. Macas, C. Messenger, P. Raffai, and R. S. de Souza, “GLADE: A galaxy catalogue for multimessenger searches in the advanced gravitational-wave detector era,” *Mon. Not. Roy. Astron. Soc.* **479** no. 2, (2018) 2374–2381, [arXiv:1804.05709 \[astro-ph.HE\]](https://arxiv.org/abs/1804.05709).

[58] **DES, NOAO Data Lab** Collaboration, T. M. C. Abbott *et al.*, “The Dark Energy Survey Data Release 1,” *Astrophys. J. Suppl.* **239** no. 2, (2018) 18, [arXiv:1801.03181 \[astro-ph.IM\]](https://arxiv.org/abs/1801.03181).

[59] R. Gray *et al.*, “Cosmological inference using gravitational wave standard sirens: A mock data analysis,” *Phys. Rev. D* **101** no. 12, (2020) 122001, [arXiv:1908.06050 \[gr-qc\]](https://arxiv.org/abs/1908.06050).

[60] S. Husa, S. Khan, M. Hannam, M. Pürrer, F. Ohme, X. J. Forteza, and A. Bohé, “Frequency-domain gravitational waves from nonprecessing black-hole binaries. I. New numerical waveforms and anatomy of the signal,” *Phys. Rev. D* **93** no. 4, (Feb., 2016) 044006, [arXiv:1508.07250 \[gr-qc\]](https://arxiv.org/abs/1508.07250).

[61] G. Ashton, M. Hübner, P. D. Lasky, C. Talbot, K. Ackley, S. Biscoveanu, Q. Chu, A. Divakarla, P. J. Easter, B. Goncharov, and et al., “BILBY: A User-friendly Bayesian Inference Library for Gravitational-wave Astronomy,” *ApJS* **241** no. 2, (Apr., 2019) 27, [arXiv:1811.02042 \[astro-ph.IM\]](https://arxiv.org/abs/1811.02042).

[62] S. Vitale, C.-J. Haster, L. Sun, B. Farr, E. Goetz, J. Kissel, and C. Cahillane, “physiCal: A physical approach to the marginalization of LIGO calibration uncertainties,” *arXiv e-prints* (Sept., 2020) arXiv:2009.10192, [arXiv:2009.10192 \[gr-qc\]](https://arxiv.org/abs/2009.10192).

[63] H.-Y. Chen, “Systematic Uncertainty of Standard Sirens from the Viewing Angle of Binary Neutron Star Inspirals,” *Phys. Rev. Lett.* **125** no. 20, (Nov., 2020) 201301, [arXiv:2006.02779 \[astro-ph.HE\]](https://arxiv.org/abs/2006.02779).

[64] C. Talbot, R. Smith, E. Thrane, and G. B. Poole, “Parallelized Inference for Gravitational-Wave Astronomy,” *Phys. Rev. D* **100** no. 4, (2019) 043030, [arXiv:1904.02863 \[astro-ph.IM\]](https://arxiv.org/abs/1904.02863).